

Light Diffusion in Multi-Layered Translucent Materials

Craig Donner

Henrik Wann Jensen

University of California, San Diego

Abstract

This paper introduces a shading model for light diffusion in multi-layered translucent materials. Previous work on diffusion in translucent materials has assumed smooth semi-infinite homogeneous materials and solved for the scattering of light using a dipole diffusion approximation. This approximation breaks down in the case of thin translucent slabs and multi-layered materials. We present a new efficient technique based on multiple dipoles to account for diffusion in thin slabs. We enhance this multipole theory to account for mismatching indices of refraction at the top and bottom of translucent slabs, and to model the effects of rough surfaces. To model multiple layers, we extend this single slab theory by convolving the diffusion profiles of the individual slabs. We account for multiple scattering between slabs by using a variant of Kubelka-Munk theory in frequency space. Our results demonstrate diffusion of light in thin slabs and multi-layered materials such as paint, paper, and human skin.

CR Categories: I.3.7 [Computing Methodologies]: Computer Graphics—Three-Dimensional Graphics and Realism

Keywords: Subsurface scattering, BSSRDF, reflection models, layered materials, diffusion theory, light transport, global illumination, realistic image synthesis

1 Introduction

Translucent materials are common in the natural world and simulating the appearance of these materials is important for realistic image synthesis. These materials come in many forms; some are homogeneous such as snow and candle wax, or may have complex internal properties such as marble and grapes, while others are composed of multiple layers such as skin and plant leaves.

Blinn [1982] was the first to simulate subsurface scattering in computer graphics in the context of dusty surfaces. Haase and Meyer [1992] used Kubelka-Munk theory to simulate scattering in paints, and Hanrahan and Krueger [1993] presented a more accurate model of single scattering in layered materials. Stam [2001] examined the total subsurface reflectance and transmittance of a slab bounded by rough surfaces. All of these models, however, assume that light scatters at a single point on the surface, and the resulting subsurface scattering is either diffuse or shaped by the scattering properties of the material.

A more complete simulation of subsurface scattering has been done using photon mapping [Dorsey et al. 1999], path tracing [Jensen et al. 1999], and scattering equations [Pharr and Hanrahan 2000]. Other Monte Carlo methods using spectral and physically based parameters [Krishnaswamy and Baranowski 2004] have also been proposed. These approaches are general and capable of simulating properties of translucent materials, but they are computationally

costly in highly scattering materials, where light diffusion dominates.

To efficiently simulate subsurface scattering in translucent materials, Jensen et al. [2001] used an analytic expression based on the dipole diffusion approximation, which assumes that the material is homogeneous and semi-infinitely thick. Although the dipole method has been modified for fast [Jensen and Buhler 2002] and interactive rendering [Mertens et al. 2003], the underlying theory has remained unchanged. Chen et al. [2004] have coupled image-based texture functions with the dipole diffusion model and photon mapping to volumetrically render thin shells covering a thick substrate, effectively obtaining a more general method for light scattering in translucent materials. The precomputation time for their method is high, however, as it relies on photon tracing.

In this paper, we extend previous work on light diffusion in translucent materials. We present a multipole diffusion approximation for light scattering in thin slabs that uses an extension to diffusion theory based on the method of images. We extend this multipole theory to account for both surface roughness and layers with varying indices of refraction, and we combine it with a novel frequency space application of Kubelka-Munk theory in order to simulate light diffusion in multi-layered translucent materials. Our method generalizes to an arbitrary number of layers, and it enables the composition of arbitrary multi-layered materials with different optical parameters for each layer. It is both accurate and efficient and easily integrated into existing implementations based on the dipole diffusion approximation.

2 Light Diffusion

The scattering of light in translucent materials is described by the Bidirectional Scattering Surface Reflectance Distribution Function (BSSRDF) [Nicodemus et al. 1977]

$$S(x_i, \vec{\omega}_i; x_o, \vec{\omega}_o) = \frac{dL(x_o, \vec{\omega}_o)}{d\Phi(x_i, \vec{\omega}_i)}. \quad (1)$$

Here L is the outgoing radiance, Φ the incident flux, x_i and $\vec{\omega}_i$ the incident position and direction, and x_o and $\vec{\omega}_o$ the exitant position and direction. In the case of highly scattering, homogeneous, and semi-infinite materials, Jensen et al. [2001] have shown that the BSSRDF can be approximated using diffusion theory, which accounts for most of the scattered light in natural materials [Jensen and Buhler 2002]

$$S_d(x_i, \vec{\omega}_i; x_o, \vec{\omega}_o) = \frac{1}{\pi} F_t(x_i, \vec{\omega}_i) R(||x_i - x_o||_2) F_t(x_o, \vec{\omega}_o). \quad (2)$$

F_t is the Fresnel transmittance at the entry and exit points x_i and x_o , and the diffuse reflectance profile, R , is approximated by a diffusion dipole

$$R(r) = \frac{\alpha' z_r (1 + \sigma_{tr} d_r) e^{-\sigma_{tr} d_r}}{4\pi d_r^3} - \frac{\alpha' z_v (1 + \sigma_{tr} d_v) e^{-\sigma_{tr} d_v}}{4\pi d_v^3}, \quad (3)$$

where $\sigma_{tr} = \sqrt{3\sigma_a \sigma_t'}$ is the effective transport coefficient, $\sigma_t' = \sigma_a + \sigma_s'$ is the reduced extinction coefficient, $\alpha' = \sigma_s'/\sigma_t'$ is the reduced albedo, and σ_a and σ_s' are the absorption and reduced scattering coefficients. $z_r = 1/\sigma_t'$ and $z_v = (1 + 4A/3)/\sigma_t'$ are the z -coordinates of the positive and negative sources relative to the surface at $z = 0$ (see Figure 1a). $r = ||x_o - x_i||_2$, and $d_r = \sqrt{r^2 + z_r^2}$ and

$d_v = \sqrt{r^2 + z_v^2}$ are the distances to the sources from a given point on the surface of the object. $D = \frac{1}{3\sigma'_t}$ is the diffusion constant and A is given by Equation (7).

The diffusion dipole is derived using a diffusion approximation of radiative transport. The diffuse radiance is approximated using a truncated spherical harmonic expansion

$$L_d(r, \vec{\omega}) = \frac{1}{4\pi} \phi(r) + \frac{3}{4\pi} \mathbf{E}(r) \cdot \vec{\omega}, \quad (4)$$

where ϕ is the fluence and \mathbf{E} is the vector flux. For a full introduction to diffusion theory and the above expression see [Ishimaru 1978]. We focus on the derivation of the dipole model from the boundary conditions to the diffusion equation. Specifically, at the surface of a material, any light that escapes is assumed to never return. Therefore, the total downward diffuse radiance at the surface into the material ($+z$ direction) is equal to the internally reflected upward diffuse radiance

$$\int_{\Omega_+} L_d(r, \vec{\omega}) (-\vec{n} \cdot \vec{\omega}) d\vec{\omega} = F_{dr} \int_{\Omega_-} L_d(r, \vec{\omega}) (\vec{n} \cdot \vec{\omega}) d\vec{\omega} \text{ at } z=0, \quad (5)$$

where Ω_+ and Ω_- indicate integration over the positive and negative hemispheres, and \vec{n} is the normal at the material surface (see Figure 1). F_{dr} is a diffuse Fresnel term that approximates the internal diffuse reflectivity of the slab. Substitution of Equation (4) into (5) and simplifying gives [Ishimaru 1978]

$$\phi(r) - 2AD \frac{\partial \phi(r)}{\partial z} = 0 \text{ at } z=0, \quad (6)$$

where D is defined as above. Note that this expression is an approximate result, but one widely held as accurate for highly scattering materials. For more rigorous conditions, see [Glasstone and Sesonske 1955]. In Equation (6), A is defined as

$$A = (1 + F_{dr}) / (1 - F_{dr}), \quad (7)$$

and represents the change in fluence due to internal reflection at the surface. The diffuse Fresnel reflectance F_{dr} can be approximated by the following polynomial expansions [Egan et al. 1973]

$$F_{dr} \simeq \begin{cases} -0.4399 + \frac{0.7099}{\eta} - \frac{0.3319}{\eta^2} + \frac{0.0636}{\eta^3}, & \eta < 1 \\ -\frac{1.4399}{\eta^2} + \frac{0.7099}{\eta} + 0.6681 + 0.0636\eta, & \eta > 1 \end{cases} \quad (8)$$

where η is the ratio of indices of refraction.

An incident beam of light is approximated by a point light source placed under x_i at a depth of one mean free path, $\ell = 1/\sigma'_t$ [Patterson et al. 1989] below the surface of the material. By Equation (6), a linear extrapolation of the fluence vanishes at $z_b = 2AD$ above the surface [Farrell and Patterson 1992], called the *extrapolation distance*. Since the positive source is embedded at ℓ , placing the negative source $(1 + 4A/3)/\sigma'_t = 2z_b + \ell$ above the surface results in zero net fluence at $-z_b$. This results in a dipole that is a good approximation of Equations (5) and (6) (see Figure 1a).

2.1 Light scattering in thin slabs

The dipole approximation was derived for the case of a semi-infinite medium. It assumes that any light entering the material will either be absorbed or return to the surface. For thin slabs this assumption breaks down as light is transmitted through the slab, which reduces the amount of light diffusing back to the surface. This means that the dipole will overestimate the reflectance of thin slabs, and it cannot correctly predict the transmittance.

We can account for light scattering in slabs by taking the changed boundary condition into account. For a slab of thickness d , we define a boundary condition for the bottom surface analogous to Equation (5). Diffuse light transmitted through the slab does not return,

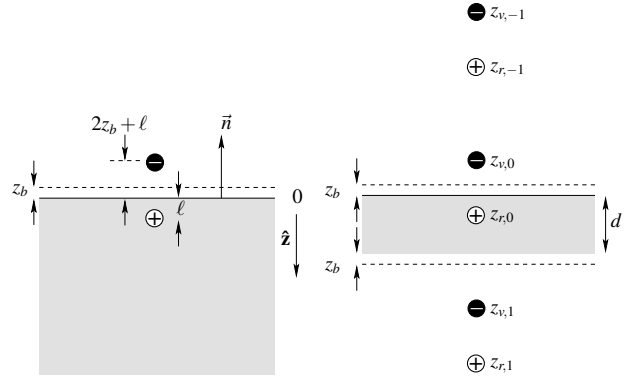


Figure 1: Dipole configuration for semi-infinite geometry (left), and the multipole configuration for thin slabs (right).

and the upward diffuse radiance is equal to the reflected downward radiance at the bottom surface

$$\int_{\Omega_-} L_d(r, \vec{\omega}) (\vec{n} \cdot \vec{\omega}) d\vec{\omega} = F_{dr} \int_{\Omega_+} L_d(r, \vec{\omega}) (-\vec{n} \cdot \vec{\omega}) d\vec{\omega} \text{ at } z=d. \quad (9)$$

Simplifying this equation gives a result similar to Equation (6),

$$\phi(r) + 2AD \frac{\partial \phi(r)}{\partial z} = 0 \text{ at } z=d, \quad (10)$$

where we make the assumption that the non-scattering mediums above and below the slab have the same index of refraction. In the next section we will show how to handle the case where the indices differ. In this case of matched boundaries, Equation (10) states that the flux vanishes at depth $d + z_b$, which is z_b below the bottom of the slab.

We can satisfy Equation (10) by mirroring the top dipole about $z = d + z_b$. The net fluence from both dipoles results in zero fluence at $z = d + z_b$ (the lower dotted line in Figure 1b) [Patterson et al. 1989]. Reinforcing the condition at $z = z_b$ (the top dotted line) requires mirroring the bottom dipole about the top line. Both boundary conditions are satisfied simultaneously only when there is an infinite array of dipoles (Figure 1b).

When the ratios of indices of refraction, and thus the extrapolation distances, are the same at both the top and bottom interfaces, the z -coordinates of the dipole sources are given by

$$\begin{aligned} z_{r,i} &= 2i(d + 2z_b) + \ell \\ z_{v,i} &= 2i(d + 2z_b) - \ell - 2z_b, \quad i = -n, \dots, n, \end{aligned} \quad (11)$$

where $2n+1$ is the number of dipoles, d is the slab thickness, and $z_b = 2AD$ is the extrapolation distance.

The reflectance due to $2n+1$ dipoles is simply the sum of their individual contributions

$$R(r) = \sum_{i=-n}^n \frac{\alpha' z_{r,i} (1 + \sigma_{tr} d_{r,i}) e^{-\sigma_{tr} d_{r,i}}}{4\pi d_{r,i}^3} - \frac{\alpha' z_{v,i} (1 + \sigma_{tr} d_{v,i}) e^{-\sigma_{tr} d_{v,i}}}{4\pi d_{v,i}^3}, \quad (12)$$

where $d_{r,i} = \sqrt{r^2 + z_{r,i}^2}$ and $d_{v,i} = \sqrt{r^2 + z_{v,i}^2}$ are the distances to the dipole sources from a given point on the surface of the object. Note that we get the dipole approximation when $n = 0$. The diffuse transmittance can be found by adjusting for the depth of the slab

$$\begin{aligned} T(r) = \sum_{i=-n}^n & \frac{\alpha' (d - z_{r,i}) (1 + \sigma_{tr} d_{r,i}) e^{-\sigma_{tr} d_{r,i}}}{4\pi d_{r,i}^3} - \\ & \frac{\alpha' (d - z_{v,i}) (1 + \sigma_{tr} d_{v,i}) e^{-\sigma_{tr} d_{v,i}}}{4\pi d_{v,i}^3}. \end{aligned} \quad (13)$$

This multipole approximation is used in the same way as the dipole.

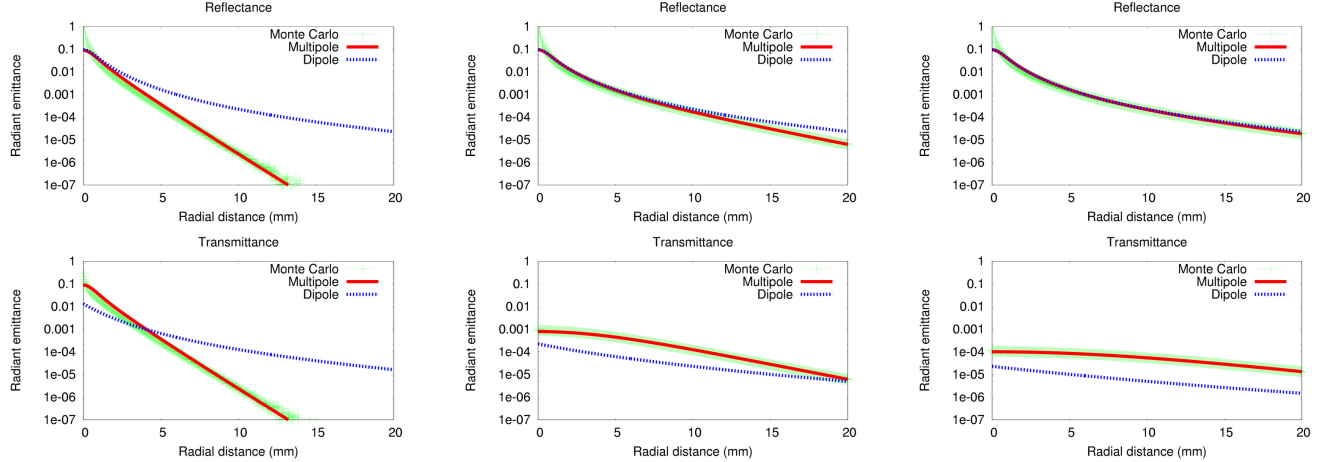


Figure 2: Comparison of the reflectance and transmission profiles of slabs of varying thickness predicted by the dipole and the multipole to Monte Carlo simulations. The slab thickness increases from 2 mean free paths in the left plot to 10 and 20 in center and right plots. The mean free path length for all three plots was 1mm.

Mfp	Total Reflectance			Total Transmittance		
	MC	Multipole	Dipole	MC	Multipole	Dipole
2	51.6%	49.8%	90.2%	49.8%	48.1%	26.5%
10	83.4%	83.8%	90.2%	13.8%	13.8%	3.0%
20	89.0%	89.0%	90.2%	6.0%	5.9%	0.7%

Table 1: Comparison of the total reflectance and transmission predicted by the dipole and multipole models compared to Monte Carlo for the plots in Figure 2.

An incident ray of light is converted into an isotropic point source embedded at depth ℓ in the slab, and the diffuse reflectance and transmittance are given by Equations (12) and (13). In practice, since the contribution of each dipole decreases with distance, the actual number required in this multipole configuration depends on the slab thickness and the optical properties of the material.

Figure 2 compares the Monte Carlo traced reflectance and transmittance of thin slabs from 2 to 20 mean free paths to the responses predicted by the dipole and multipole methods. The dipole transmittance is calculated using the linear distance from the incident light to exitant location (i.e. assuming the points are on the same surface). Note that because the dipole does not account for light that exits the bottom of the slab, it predicts light will continue to scatter and exit the top of the material. For thicker slabs, the dipole performs well, but is noticeably divergent for thin slabs. The dipole also incorrectly predicts both the intensity and shape of the transmittance profiles in all cases. The multipole accurately predicts both the reflectance and transmittance in all cases. This is also evident in the total reflectance and transmittance predicted by the two models (Table 1).

2.2 Refractive index mismatches

The multipole approximation has been used to compute reflectance and transmittance from slabs in the space and time domains [Contini et al. 1997; Wang 1998], but only when the non-scattering materials above and below the slab are assumed to have the same index of refraction. When dealing with multi-layered materials, however, this is not always the case. Many materials (e.g. skin, plant leaves), are composed of layers with differing indices of refraction.

Recall that the multipole must satisfy both boundary equations (6) and (10) simultaneously. When the index of refraction ratios at the two interfaces of the slab differ, the difference in Fresnel reflectance

generate different conditions at the top and the bottom of the slab

$$\phi(r) - 2A(0)D \frac{\partial \phi(r)}{\partial z} = 0, \quad \text{at } z = 0, \quad (14)$$

$$\phi(r) + 2A(d)D \frac{\partial \phi(r)}{\partial z} = 0, \quad \text{at } z = d, \quad (15)$$

where $A(0)$ and $A(d)$ (see Equation (7)) are calculated using the diffuse Fresnel reflectance at the top and bottom interfaces. These two conditions will give different vanishing points for the fluence. Satisfying both conditions at once requires adjusting the mirroring distance of the dipoles about the slab

$$\begin{aligned} z_{r,i} &= 2i(d + z_b(0) + z_b(d)) + \ell \\ z_{v,i} &= 2i(d + z_b(0) + z_b(d)) - \ell - 2z_b(0), \end{aligned} \quad (16)$$

where each z_b is computed using the appropriate A . When the Fresnel reflectances are the same, $A(0) = A(d)$, and the formulas in Equation (16) simplify to those in Equation (11).

2.3 Diffusion in multi-layered materials

Until now, the multipole method has not been applied to multi-layered materials. Previous work in the medical physics community related to light scattering through layered media have focused on solving boundary conditions at an interface between these scattering layers [Keijzer et al. 1988]. These conditions lead to non-analytic solutions that have no clear extension to more than two or three layers. They also do not directly provide the steady-state reflectance and transmittance profiles that are useful for rendering.

In this section, we present a novel method for approximating the steady-state reflectance and transmittance profiles of multi-layered materials by combining the multipole method with Kubelka-Munk theory.

Given the incident flux $\Phi(x, y, \vec{\omega})$ at a surface, we can compute the radiant emittance profile, M , through the slab at (x, y) by convolving the incident flux, Φ , with the transmittance profile, T

$$M(r) = \int_{-\infty}^{\infty} \int_{-\infty}^{\infty} \Phi(x', y', \vec{\omega}) T(r'') dx' dy' = \Phi(x, y, \vec{\omega}) * T(r), \quad (17)$$

where $r'' = \sqrt{(x - x')^2 + (y - y')^2}$.

Both the dipole and multipole methods assume that the emitted light is diffuse. They also assume that the angle of incidence has no effect on the reflection or transmission response of a material. This

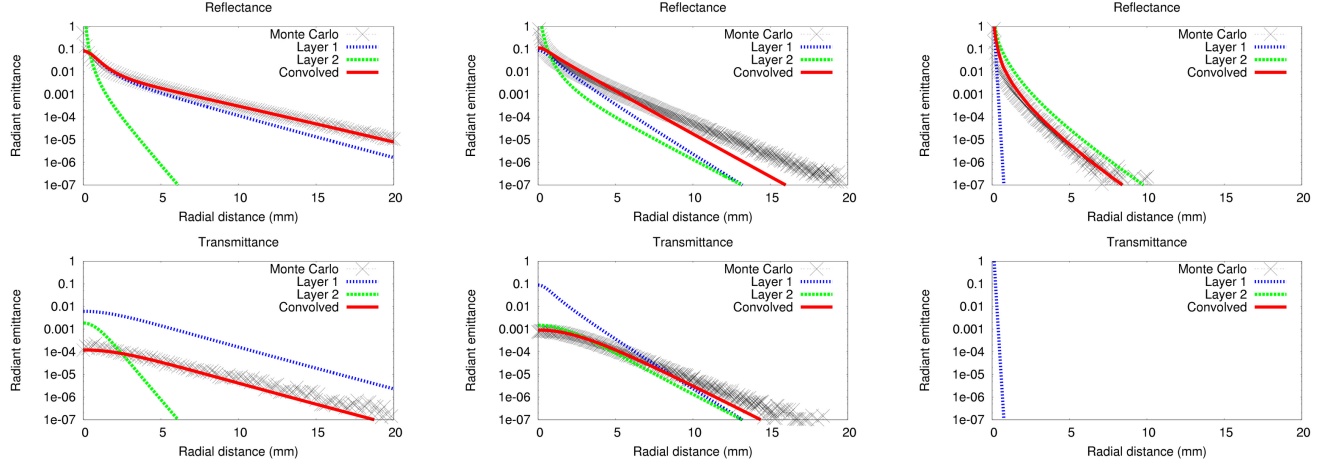


Figure 3: The convolution technique is robust for a wide range of parameters. Our method is most accurate near the source, where accuracy is most important. (left) A thick low-scattering top layer covering a highly scattering thinner lower layer. (middle) A thin low-scattering top layer over a highly scattering thin bottom. (right) A thin highly scattering top layer over a very thick substrate. There is no transmittance since it is optically thick.

Material	Reflectance			Transmittance		
	MC	KM	no-KM	MC	KM	no-KM
Figure 3 left	85.1%	81.4%	65.6%	1.15%	0.90%	0.42%
Figure 3 middle	94.8%	97.8%	71.5%	3.5%	3.5%	8.4%
Figure 3 right	82.1%	78.0%	67.9%	0.0%	0.0%	0.0%

Table 2: Comparison of the total reflectance and transmission predicted by the multipole models to Monte Carlo for the materials in Figure 3, with and without the correction described in Section 2.3.

effectively equates the impulse response of a slab to its diffuse response. Note that the multipole gives the impulse response of a slab.

We can combine the profiles of two different layers by assuming that all interactions between the two layers are due to multiple scattering. This assumption is reasonably accurate as long as diffusion theory is applicable to the individual layers — i.e. they have a thickness of at least a few mean free paths. Based on this assumption, we can compute the profile T_{12} of the light transmitted through two slabs with transmittance profiles T_1 and T_2 by convolving the profiles

$$T_{12}(r) = \int_{-\infty}^{\infty} \int_{-\infty}^{\infty} T_1(r') T_2(r'') dx' dy' = T_1(r) * T_2(r), \quad (18)$$

where $r' = \sqrt{x'^2 + y'^2}$. This equation assumes that light transmitted through layer 1 onto layer 2 is transmitted through layer 2. This is not entirely correct, since some of the light may transmit through layer 1, and later return to layer 1 after scattering in layer 2. This light can again scatter back to layer 2 and transmit out the bottom of the slab. To account for these additional scattering events at the interface we correct Equation (18) by additional terms accounting for each scattering event:

$$T_{12} = T_1 * T_2 + T_1 * R_2 * R_1 * T_2 + T_1 * R_2 * R_1 * R_2 * R_1 * T_2 + \dots \quad (19)$$

where we have omitted the dependence on r for brevity. This series of convolutions can be evaluated efficiently using Fourier theory, which changes each convolution into a product in frequency space

$$\begin{aligned} \mathcal{T}_{12} &= \mathcal{T}_1 \mathcal{T}_2 + \mathcal{T}_1 \mathcal{R}_2 \mathcal{R}_1 \mathcal{T}_2 + \mathcal{T}_1 \mathcal{R}_2 \mathcal{R}_1 \mathcal{R}_2 \mathcal{R}_1 \mathcal{T}_2 + \dots \\ &= \mathcal{T}_1 \mathcal{T}_2 (1 + \mathcal{R}_2 \mathcal{R}_1 + (\mathcal{R}_2 \mathcal{R}_1)^2 + (\mathcal{R}_2 \mathcal{R}_1)^3 + \dots), \end{aligned} \quad (20)$$

where \mathcal{R} and \mathcal{T} are Fourier transformed diffuse reflectance and

transmittance profiles. The resulting expression is a geometric series. Assuming that $\mathcal{R}_1 \mathcal{R}_2 < 1$, we can simplify Equation 20 to

$$\mathcal{T}_{12} = \frac{\mathcal{T}_1 \mathcal{T}_2}{1 - \mathcal{R}_2 \mathcal{R}_1}. \quad (21)$$

A similar analysis to above produces a similar formula for the reflectance of two layers

$$\mathcal{R}_{12} = \mathcal{R}_1 + \frac{\mathcal{T}_1 \mathcal{R}_2 \mathcal{T}_1}{1 - \mathcal{R}_2 \mathcal{R}_1}. \quad (22)$$

This method can be extended to more than two layers by recursive substitution of Equations (21) and (22) in for \mathcal{R}_1 or \mathcal{T}_1 , and re-evaluating the formulas. The real-space reflectance and transmittance profiles of a many-layered material is computed by computing the inverse Fourier transform of the total frequency response.

Note that these formulas are identical to Kubelka's [1954], but applied in frequency space. They can also be considered as an application of the multipole approximation as a scattering function in operator form [Pharr and Hanrahan 2000].

Figure 3 compares the convolution of the responses of two-layered materials, and a comparison to Monte Carlo photon tracing. The convolution of the two layers closely approximates the reflectance and transmittance profiles near the source, and though it can diverge slightly far from the source, the intensity levels are not significant. Table 2 shows the effect of frequency space correction. Note that with correction, the total reflectance and transmittance profiles more closely matches the Monte Carlo simulations.

2.4 Rough surfaces

Our derivation so far has assumed that the top surface of the material is smooth. We can account for rough surfaces by modifying the boundary condition that states how the diffused light is reflected at the surface. This can be done by replacing the Fresnel term in Equation (5) by an appropriate BRDF. In the following, we will assume that a microfacet model can be used to describe the roughness of the surface, and we model the surface reflection using a Torrance-Sparrow BRDF [Torrance and Sparrow 1967]

$$f_r(x, \vec{\omega}_o, \vec{\omega}_i) = \frac{D(x, \vec{\omega}_o, \vec{\omega}_i) G(x, \vec{\omega}_o, \vec{\omega}_i) F(x, \vec{\omega}_i, \vec{\omega}_o)}{4(\vec{\omega}_i \cdot \vec{n})(\vec{\omega}_o \cdot \vec{n})}, \quad (23)$$

where \vec{n} is the surface normal, and D , G , and F are the facet distribution, geometric term, and the Fresnel term (see [Glassner 1995] for details). In the case of a smooth surface the diffuse Fresnel term, F_{dr} , given in Equation (8) specifies the fraction of diffuse light reflected at the surface. In the case of a rough surface we replace this term by an average diffuse reflection, ρ_d . For the Torrance-Sparrow model there is no analytic approximation of the diffuse reflection, and we compute it using Monte Carlo sampling by evaluating the BRDF for random diffuse incident directions and averaging the resulting value for the reflection (this is done once for a given material).

Once the diffuse reflection factor, ρ_d , is computed we can modify the A term (Equation 7) used in the computation of the extrapolation distance as follows:

$$A = \frac{1 + \rho_d}{1 - \rho_d}. \quad (24)$$

In addition, Equation (2) is changed by replacing both Fresnel terms with a diffuse transmission function

$$S_d(x_i, \vec{\omega}_i; x_o, \vec{\omega}_o) = \frac{1}{\pi} \rho_{dt}(x_i, \vec{\omega}_i) R(||x_i - x_o||) \rho_{dt}(x_o, \vec{\omega}_o), \quad (25)$$

where

$$\rho_{dt}(x, \vec{\omega}_o) = 1.0 - \int_{2\pi} f_r(x, \vec{\omega}_o, \vec{\omega}_i) (\vec{\omega}_i \cdot \vec{n}) d\vec{\omega}_i. \quad (26)$$

We assume all light that is not reflected by the BRDF model is transmitted into the material. Since ρ_{dt} is a fairly smooth function, we use numerical integration and generate a small table for different incoming angles. The use of ρ_{dt} is an approximation, as the transmitted light has a directional distribution described by a BRDF for transmitted light [Stam 2001]. Since we use a diffusion model, however, this distribution can be ignored, and we consider all transmitted light to be diffuse.

The final model for the appearance of a rough translucent material consists of the diffusion model plus the BRDF for the reflection of light by the rough surface. As the surface roughness increases this model predicts that less light will be transmitted into the material, while more light is reflected directly by the surface. This results in a desaturation of the color of the translucent material as the importance of the (often white) surface reflection grows.

3 Rendering with the Multi-Layer Model

The multi-layered diffusion model is computed by evaluating the multipole for each layer, and using the Fourier transform technique described in the previous section to obtain the total diffuse transmittance and reflectance of the material. Because no analytical transform of the multipole equation exists, we use the discrete Fourier transform to generate tabulated reflectance and transmittance profiles. Discretely sampling the profiles is computational efficient compared to re-evaluating the multipole for every pixel. This is particularly beneficial when capturing the properties of highly scattering extremely thin layers, where a large number of dipole pairs may be required. For thicker, less scattering single slabs, the analytic multipole model can be used directly. Both the analytic multipole and the tabulated profiles can be rendered using the same techniques as the dipole method.

The multi-layer model provides both a reflectance and a transmittance profile, but the geometry to be rendered determines how they should be used. As with the dipole model these profiles are only valid for planar slabs, and can only be used as approximations for other types of geometry. When modeling a multi-layered material such as skin it is sufficient in most cases to use only the reflectance profile to model the diffusion of light. In the case of complex thin

(a few mean-free paths) geometry it is possible to blend the reflection and transmission profiles, depending on the normals \vec{n}_l and \vec{n}_s at the location of the incident light and the point being shaded

$$P_d(r) = \frac{1}{2}(\vec{n}_s \cdot \vec{n}_l + 1)R_d(r) + \frac{1}{2}(1 - \vec{n}_s \cdot \vec{n}_l)T_d(r). \quad (27)$$

This equation computes a new profile as the weighted average of the reflected and transmitted profiles. Note that only the reflected profile is used if the normals point in the same direction, while only the transmitted profile is used if they point in opposite directions. One potential improvement to this formula would be to take into account the relative position of the two points as well (e.g. if the normals are facing each other). However, since the geometry between the point being shaded and the point being illuminated is unknown, there is no guarantee of accuracy. For applications that require high degrees of precision for small complex geometry, it is better to use Monte Carlo photon tracing or a multi-grid diffusion solver.

3.1 Texturing

Texturing a multi-layered translucent material can be done in a number of ways. If the texture contains information about the scattering properties of each layer then it is possible to approximate the spatially varying reflectance and transmittance profiles by convolving the spatially varying reflectance and/or transmittance profiles for the individual layers (assuming that the surface is locally homogeneous). This process is costly as it has to be done for every point on the surface or for every texture element.

A simpler technique that works well in practice is to assume that the texture is given as an albedo map (e.g. diffuse reflectance) similar to textures used to shade opaque materials. This approach has been used on translucent materials based on the dipole model [Jensen and Buhler 2002; Hery 2003]. If we further assume that only nearby texture values influence each other then we can account for texturing using the following approach.

- First, we convolve the texture with the reflectance profile (and the transmittance profile if thin geometry is being shaded). This effectively blurs the texture according to the diffusion of light (a similar approach has been used on the irradiance value by Borshukov et al. [2003]).
- Next, we normalize the texture such that the average is a white color. This is done to ensure that the color of the diffusion process is used, rather than the texture color. If the texture color is important then the texture can be normalized by the reflectance and/or transmittance value predicted by the multipole method (we have not used this approach).
- Finally, during rendering we compute the effective diffusion of light using the reflectance and/or transmittance profile, and scale the predicted radiant emittance by the normalized texture value.

4 Results and Discussion

We have implemented the multi-layered diffusion model in a Monte Carlo ray tracer that supports direct sampling of scattering profiles as described in [Jensen et al. 2001]. The images were rendered on a 2.8GHz Pentium IV, and the rendering times for the individual images were from one to five minutes. Preprocessing time to generate the scattering profiles ranged from five seconds to under one second, using 1000 dipole pairs to ensure accuracy.

Figure 4 compares the accuracy of the multipole method with the dipole method and Monte Carlo photon tracing. The scene contains a thin piece of parchment illuminated from behind. The parchment is roughly 1 mm. thick, which corresponds to approximately four mean free paths. The dipole predicts a transmittance of about 3.3% compared with 22.6% for the multipole and 21.5% for the Monte



Figure 4: A piece of parchment illuminated from behind. Note, how the dipole model (left) underestimates the amount of transmitted light, while the multipole model (middle) matches the reference image computed using Monte Carlo photon tracing (right).



Figure 5: A buddha statuette sprayed with a thin layer of white paint. The first and third images are front-lit, the second and fourth back-lit.

Carlo reference result. As a consequence, the parchment is too dark when rendered with the dipole diffusion model, while the multipole model more precisely predicts the correct appearance.

Figure 5 shows the effect of adding a thin layer of paint onto a thicker buddha statue made of jade. The paint is highly scattering of white light, while the jade absorbs most non-green light. Adding the paint layer causes the reflected light to become more white, and attenuates the amount of light that reaches the jade, causing the statue to look more opaque. The transmitted light, however, remains green as it still scatters through the jade material.

Figure 7 demonstrates several renderings of a marble statue with different surface roughness values. As the surface roughness increases, the surface changes from having an oily appearance to looking more dry and rough. Another important change is the desaturation of the color of the statue due to an increase in the amount of reflected light, and a reduction in the amount of lighting due to subsurface scattering.

Figure 6 displays renderings of a leaf composed of a thick absorbing layer over a thin highly scattering layer, similar to [Hemenger 1977], with absorption parameters taken from [Fukshansky et al. 1993]. Note that while the orientation of the leaf affects the reflectance, the transmittance is nearly the same. This bicoloration is an important visual element of many leaves. For the leaf model, we applied both thickness and bump maps on the geometry to simulate the appearance of the leaf veins. The thickness map is effectively used as a displacement map, which increases the distance of the diffused lighting. This gives the effect of thickness, but it is only an approximation as the overall reflectance profile changes as a function of the thickness of each layer. The leaf color is caused by multiple scattering; no textures have been used.

Multiple layered models have been shown to be effective in simulating the optical properties of human skin [Tuchin 2000]. In Figure 8 we demonstrate a three layer model of human skin applied to a high-resolution digital scan of a head. No bump map was used;



Front and back, frontlit. Front and back, backlit.

Figure 6: A layered leaf lit from front and behind. The reflectance of the front and back sides of the leaf differ significantly, while the transmittance is nearly identical. Note that the color is due to multiple scattering; no textures are applied.

	σ_a (mm^{-1})			σ_s (mm^{-1})			η	g	d (mm)
	R	G	B	R	G	B			
epidermis	2.1	2.1	5.0	48.0	60.0	65.0	1.4	0.0	.03
upper dermis	0.16	0.19	0.30	32.0	40.0	46.0	1.34	0.25	.05
bloody dermis	0.085	1.0	25.0	4.5	4.7	4.8	1.4	0.8	∞

Table 3: Optical parameters used in generating the images in Figure 8. η is the index of refraction, and d is the thickness of the layer.

the surface detail is due to the actual geometry of the model. The parameters for each layer are from Tuchin [2000] and summarized in Table 3. The top images show the contribution each layer gives to the overall appearance, as well as the contribution of surface roughness at the top surface of the skin. The lower images add texturing as described in the previous section. Note that although the individual layers may not appear to be skin-like, this is often the case of actual photographs of the bloodless top layers of human skin. Also, it is the overall reflectance from the convolution of these layers that gives the final appearance. The bloody dermis layer is assumed to be semi-infinite, which is often done to simulate the effects of internal tissues, while the highly scattering upper layers determine the softness and tint of the skin. Figure 8 shows a comparison between the multilayer model and the dipole model using the parameters provided in [Jensen et al. 2001]. The dipole overestimates the amount of scattering, giving the face a waxy, translucent look that blurs the features of the skin. The multi-layered model results in a less blurry appearance due to the improved approximation of the highly scattering epidermal and dermal layers compared with the bloody dermis. The overall appearance of the skin is still translucent as can be seen when the light is bleeding into shadowed regions, or when the skin is illuminated from behind (e.g. at the ear).

Note that parameters to the dipole model cannot always be used in the multipole model directly, as the dipole parameters are designed to capture the overall appearance of a semi-infinite sample of the material. Instead, the images in Figure 8 have been rendered using parameters from existing work in tissue optics. These parameters are more intuitive than the parameters in the dipole model, since the specific properties of each layer can be modified (e.g. blood concentration or melanin) to change the overall appearance.

5 Conclusions and Future Work

We have presented an efficient method for accurately rendering thin and multi-layered translucent materials based on a multipole diffusion approximation. The multipole theory is enhanced to account for mismatched indices of refraction as well as rough surfaces. Using a novel application of Kubelka-Munk theory in frequency space a new method for combining multiple layers of translucent materials has been introduced. The new model is efficient and accurate, and it renders thin and layered materials such as paper and skin faithfully. In the future we would like to extend the diffusion theory to objects with internal structures and to investigate if the multi-layer model can be used to make accurate measurements of subsurface scattering in layered translucent materials.



Figure 7: A translucent marble statue with surface roughness 0.1 on the left, 0.5 in the middle, and 1.0 on the right. The smaller images show the subsurface scattering component and the roughness component of the smooth (0.1) and the rough (1.0) translucent statues. Note how the smooth version is more shiny and brighter due to a higher subsurface scattering component. As the surface gets more rough the surface reflection increases, which reduces the amount of subsurface scattering, and the overall result is a desaturation of the color of the marble material.

6 Acknowledgments

Special thanks to XYZRGB for providing the high resolution 3D scans of the face and paper models, to Alexandra Pham and Aiko Kitagawa for their suggestions regarding skin rendering, and to Arash Keshmirian for modeling the leaf. Thanks to the SIGGRAPH reviewers, Sameer Agarwala, and Josh Wills for helpful comments. The buddha model was provided by The Stanford 3D Scanning Repository. This research was supported by a Sloan Fellowship and the National Science Foundation under Grant No. 0305399. The first author was partially funded by a grant from CalIT².

References

- BLINN, J. F. 1982. Light reflection functions for simulation of clouds and dusty surfaces. In *Computer Graphics (Proceedings of ACM SIGGRAPH 1982)*, ACM, vol. 16, 21–29.
- BORSHUKOV, G., AND LEWIS, J. P. 2003. Realistic human face rendering for “The Matrix Reloaded”. In *ACM SIGGRAPH 2003 Sketches & Applications*, ACM, 1.
- CHEN, Y., TONG, X., WANG, J., LIN, S., GUO, B., AND SHUM, H.-Y. 2004. Shell texture functions. *ACM Trans. Graphic.* 23, 343–353.
- CONTINI, D., MARTELLI, F., AND ZACCANTI, G. 1997. Photon migration through a turbid slab described by a model based on diffusion approximation. I. Theory. *Appl. Opt.* 36, 19, 4587–4599.
- DORSEY, J., EDELMAN, A., JENSEN, H. W., LEGAKIS, J., AND PEDERSEN, H. K. 1999. Modeling and rendering of weathered stone. In *Proceedings of ACM SIGGRAPH 1999*, ACM Press/Addison-Wesley Publishing Co., New York, Computer Graphics Proceedings, 225–234.
- EGAN, W. G., HILGEMAN, T. W., AND REICHMAN, J. 1973. Determination of absorption and scattering coefficients for nonhomogeneous media. 2: Experiment. *Appl. Opt.* 12, 1816–1823.
- FARRELL, T. J., AND PATTERSON, M. S. 1992. A diffusion theory model of spatially resolved, steady-state diffuse reflections for the noninvasive determination of tissue optical properties *in vivo*. *Med. Phys.* 19, 4, 879–888.
- FUKSHANSKY, L., VON REMISOKSKY, A. M., AND MCCLENDON, J. 1993. Absorption spectra of leaves corrected for scattering and distributional error: a radiative transfer and absorption statistics treatment. *Photochem. Photobiol.* 57, 3, 538–555.
- GLASSNER, A. S. 1995. *Principles of Digital Image Synthesis*. Morgan Kaufmann.
- GLASSTONE, S., AND SESONSKE, A. 1955. *Nuclear Reactor Engineering*. Van Nostrand Company.
- HAASE, C. S., AND MEYER, G. W. 1992. Modeling pigmented materials for realistic image synthesis. *ACM Trans. Graphic.* 11, 4, 305–335.
- HANRAHAN, P., AND KRUEGER, W. 1993. Reflection from layered surfaces due to subsurface scattering. In *Proceedings of ACM SIGGRAPH 1999*, ACM Press/Addison-Wesley Publishing Co., New York, Computer Graphics Proceedings, 164–174.
- HEMENERG, R. P. 1977. Optical properties of turbid media with specularly reflecting boundaries: applications to biological problems. *Appl. Opt.* 16, 7, 2007–2012.
- HERY, C. 2003. Implementing a skin bsrdf. *ACM SIGGRAPH 2003 Course 9*, 73–88.
- ISHIMARU, A. 1978. *Wave Propagation and Scattering in Random Media*. Oxford University Press.
- JENSEN, H. W., AND BUHLER, J. 2002. A rapid hierarchical rendering technique for translucent materials. *ACM Trans. Graphic.* 21, 576–581.
- JENSEN, H. W., LEGAKIS, J., AND DORSEY, J. 1999. Rendering of wet materials. In *Rendering Techniques '99*, 273–282.
- JENSEN, H. W., MARSCHNER, S. R., LEVOY, M., AND HANRAHAN, P. 2001. A practical model for subsurface light transport. In *Proceedings of ACM SIGGRAPH 2001*, ACM Press/Addison-Wesley Publishing Co., New York, Computer Graphics Proceedings, 511–518.
- KEIJZER, M., STAR, W. M., AND STORCHI, P. R. M. 1988. Optical diffusion in layered media. *Appl. Opt.* 27, 9, 1820–1824.
- KRISHNASWAMY, A., AND BARONOSKI, G. V. G. 2004. A biophysically-based spectral model of light interaction with human skin. In *Proceedings of EUROGRAPHICS 2004*, vol. 23.
- KUBELKA, P. 1954. New contributions to the optics of intensely light-scattering materials. part ii: Non homogeneous layers. *J. Opt. Soc. Am.* 44, 4, 330–335.
- MERTENS, T., KAUTZ, J., BEKAERT, P., SEIDEL, H.-P., AND REETH, F. V. 2003. Interactive rendering of translucent deformable objects. In *Proceedings of the 14th Eurographics Workshop on Rendering*, 130–140.
- NICODEMUS, F. E., RICHMOND, J. C., HSIA, J. J., GINSBERG, I. W., AND LIMPERIS, T. 1977. *Geometrical Considerations and Nomenclature for Reflectance*. National Bureau of Standards.
- PATTERSON, M. S., CHANCE, B., AND WILSON, B. C. 1989. Time resolved reflectance and transmittance for the noninvasive measurement of tissue optical properties. *Appl. Opt.* 28, 12, 2331–2336.
- PHARR, M., AND HANRAHAN, P. 2000. Monte carlo evaluation of non-linear scattering equations for subsurface reflection. In *Proceedings of ACM SIGGRAPH 2000*, ACM Press/Addison-Wesley Publishing Co., New York, Computer Graphics Proceedings, 75–84.
- STAM, J. 2001. An illumination model for a skin layer bounded by rough surfaces. In *Proceedings of the 12th Eurographics Workshop on Rendering*, 39–52.
- TORRANCE, K. E., AND SPARROW, E. M. 1967. Theory for off-specular reflection from roughened surfaces. *J. Opt. Soc. Am.* 57, 1105–1114.
- TUCHIN, V. 2000. *Tissue Optics: Light Scattering Methods and Instruments for Medical Diagnosis*. SPIE Press.
- WANG, L. V. 1998. Rapid modeling of diffuse reflectance of light in turbid slabs. *J. Opt. Soc. Am. A* 15, 4, 936–944.

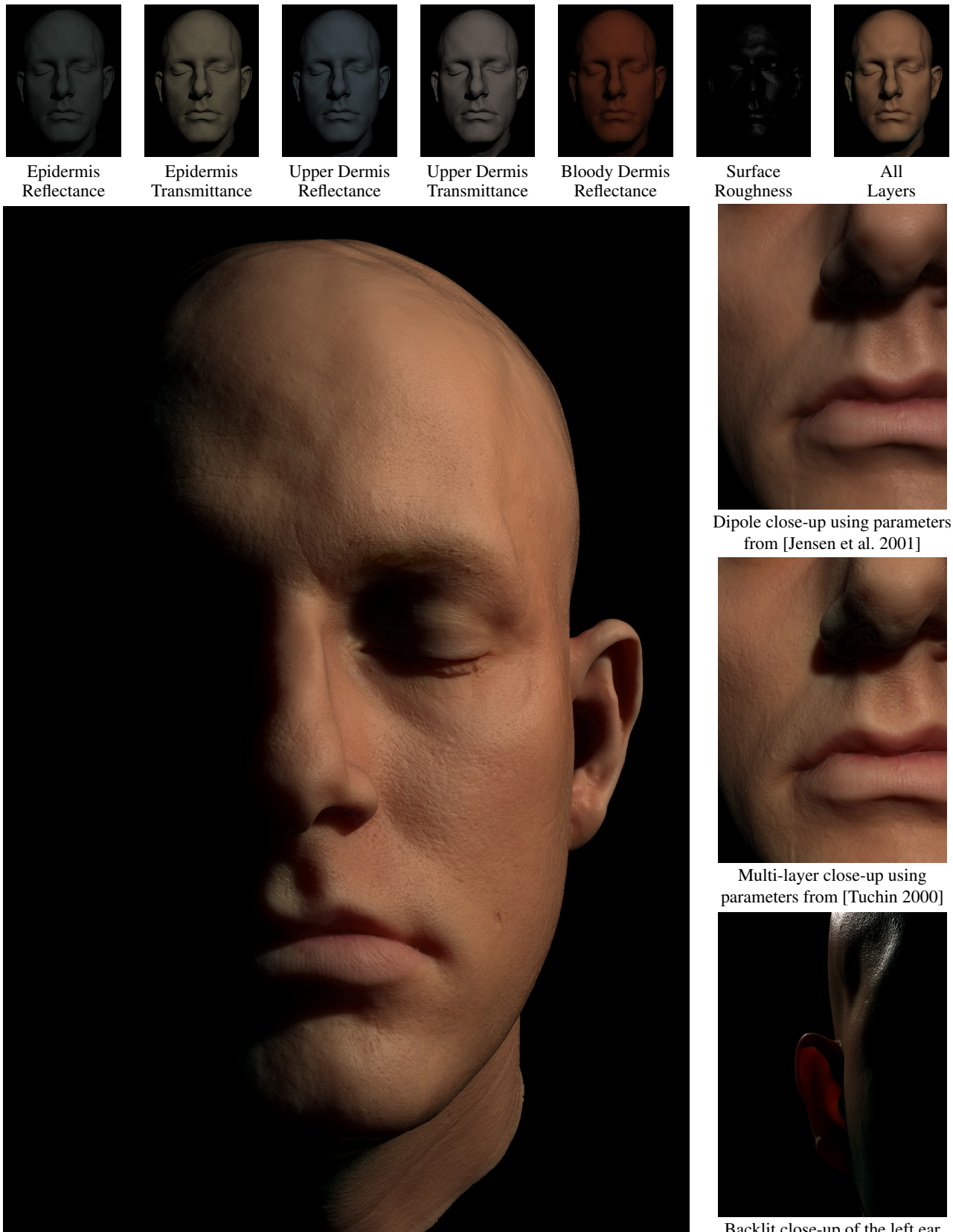


Figure 8: A multi-layered model of human skin using measured parameters for the individual skin layers [Tuchin 2000]. The top images show the reflectance and transmittance of the epidermis, upper dermis, and the bloody dermis layers. The far right image shows the combination of these layers using the multi-layer model. The middle images on the right compares the dipole model using the parameters from [Jensen et al. 2001] with the multi-layer model. Note how the combination of the different layers results in skin that captures both the translucency of the bloody dermis as well as the localized scattering in the epidermis. The lower right image shows light scattering through the backlit ear.